DEPARTMENT OF MARINE SCIENCES

CHARACTERIZATION OF WAVE ENERGY POTENTIAL AT ISLANDSBERG

Cecilia Gustafsson

Degree project for Master of Science (120 hp) with a major in Physical Oceanography
MAR601, Degree Project for Master in Marine Sciences: physical oceanography, 45 hp
Second Cycle

Semester/year:	Spring/Summer 2017
Supervisor:	Martin Johnsson, DHI, Jens Engström, Division of Electricity (Uppsala University), and Torsten Linders, Department of Marine Sciences (University of Gothenburg)
Examiner:	Göran Björk, Department of Marine Sciences

Characterization of wave energy potential at Islandsberg

Cecilia Gustafsson

13th November 2017

Abstract

A detailed study of the wave climate offshore of Islandsberg, on the Swedish west coast, was carried out to describe the spatial and temporal distribution of wave characteristics. Wave data were established for 5 years (2005-2009) through numerical modelling using the MIKE 21 Spectral Wave model (courtesy of DHI). The Islandsberg set-up of the model is shown to resolve key wave parameters well compared to observations. A higher maximum wave height was estimated during the storm Gudrun (January 2005) than the highest statistical 100 year wave estimated in an earlier study. The present study shows the importance of a long time perspective when characterizing waves. It also supports a detailed spatial resolution when describing waves to e.g. evaluate sites for marine installations. The established local spectral wave parameters at Islandsberg can be further analyzed in future projects.

1 Introduction

Ocean waves can provide a local source of energy in coastal communities. The characterization of wave energy potential is important for investigating potential sites for installations of wave power plants. Choosing the optimal wave energy converter (WEC) for a site also demands knowledge of the local wave energy characteristics. The prevailing waves at a location wear on all types of marine structures, and therefore condition the lifespan at sea. Erosion or deposit of bottom material is also affected by wave conditions, which in turn affects marine eco-systems.

Marine installations needs to resist harsh conditions regarding winds, waves and currents, as well as biofouling. Off shore test sites (areas intended for testing prototypes in the field) allow for evaluation of the robustness of new technology, and its impact on the surroundings. Marine inventions that can benefit from tests at such sites can be measurement systems, underwater robotics, wind- and wave energy converters etc.

At the marine test site at Islandsberg, on the Swedish west coast, research on wave climate and WECs is being conducted by the Division of Electricity, Uppsala University. The research and development on-site includes wave climate analysis, WEC testing and studies of environmental impact (www.teknik.uu.se).

The study presented in this report aims to further characterize the wave energy potential in the local area at, and surrounding, the Islandsberg test site. The first part of the report gives an introduction to ocean wave energy, the Islandsberg test site and a detailed description of the aim of characterizing the wave energy potential at Islandsberg. Also, different designs of WECs are briefly introduced. The following parts gives (2) the methodology, (3) results, (4) discussion and conclusions of this characterization of the Islandsberg wave conditions. As mentioned above, wave characteristics are important for other coastal concerns than WECs. However, the focus here will be from a WEC perspective, since the Islandsberg test site is accessible for inventors in marine renewable energy.

1.1 The energy in surface waves

At areas where wind can blow freely along the sea surface, without interruption of land or islands, the wind is said to have "fetch". At such stretches of open ocean, there is potential for generation of large waves. Scotland and Norway are two examples were high waves are expected to arrive at the coast. The west coast of Sweden, at least the northern part of it, is also exposed to a long fetch stretching out to the North Sea, see Fig.1a.

At mid-latitudes winds are relatively strong, giving a regional potential energy resource from both wind and waves. Ocean waves in a fully developed sea, however, can give up to 5 times the power flow intensity as the wind that generated them (Falnes, 2007). At latitudes 40-50^o, offshore storm seas can contain wave power levels reaching several MW/m (Falnes, 2007).

A few reported estimates of global potential of wind and water energy sources are given in Tab. 1. The estimates in Tab. 1 describe possible electricity production from such energy sources, rather than the total energy content of the resource.

Waves on the Swedish coasts provides an energy resource of 5-10 TWh/yr (Clément et al., 2002). The Swedish net production of electricity was 158.9 TWh in 2015 (Energimyndigheten, 2016).

On the west coast of Sweden, waves contains most energy during the stormy seasons of fall and winter (Waters, Engström, Isberg, and Leijon, 2009), coinciding with cold temperatures and a higher demand of energy for heating. Powerful sea states, however, dictates careful dimensioning of WECs for the construction to function and survive in such wave conditions.

The energy absorbed from the wind by waves propagates with the wave group velocity, until the energy dissipates. The dissipation of wave energy occurs by many processes, such as white-capping, bottom interaction and breaking when waves reach the shore.

Table 1: Estimates of potential global effect produced from wind, wave and water motion, as listed in literature.

Energy source	Global potential [TW]	
	Pelc and Fujita, 2002	Rogner et al., 2012
Ocean waves	2	
Tidal energy	0.06 - 0.1	
Offshore wind	> 0.1	
Onshore wind		2 - 11
Hydropower		1-6

1.2 The marine test site at Islandsberg

The Islandsberg test site was initiated in 2004 by the Division of Electricity, Uppsala University, for research on WECs (Leijon et al., 2008). The tests at the site includes full-scale experiments on WECs and marine substations (Waters et al., 2011) and environmental studies such as WEC effect on bottom fauna (Langhamer, 2010).

The site is located southwest of the town Lysekil on the Swedish west coast (see Fig. 1a). It is part of the European network Marinet 2, a collaboration opening up access to test facilities to increase the development of marine renewable energy technologies (Ocean Energy Europe, 2017). A sea chart with markings of the Islandsberg test site is given in Fig. 1b. Two markers on the sea chart marks the previous north-south extension of the site. The northern marker is placed at 58°11.850′ N, 11°22.460′ E, about 2 km off the coast at Islandsberg. The present test site area is visualized by the red line in Fig. 1b.

The waves are recorded on-site by a wave measurement buoy (Datawell Waverider$^{\text{TM}}$), that measures the sea surface elevation at 2.56 Hz. The observed wave climate is relatively mild, with typical wave energy periods of $T_E = 4$ s and significant wave heights $H_S < 0.5$ m (Leijon et al., 2008). Such gentle sea states are not optimal for commercial wave energy farming. However, the somewhat calm wave conditions together with the proximity to marine research facilities and the limited depth allowing for diving, made the site interesting for testing and developing WECs (Leijon et al., 2008).

The site is relatively open to the west, allowing offshore generated waves to propagate towards the test site unhindered. Sheltering islands and shallow depths are spread out mainly to the north and south of the site, locally preventing wind generation of waves and wave propagation in the N-S direction.

The depth is 25 m at the offshore end of the site, slightly decreasing shoreward to 24 m. The bottom material is mostly sandy silt (Cato and Kjellin, 2008).

1.3 Observed and modelled waves

To characterize the wave climate, including rough sea states produced by storms, one needs long time series of wave data. For a specific region such data might not be available. Instead, models can be used to simulate wave conditions from wind data (e.g. Komen et al., 1994). In this way, knowledge of the local historical wind field can give an estimate of the local wave characteristics - a *hindcast* wave model.

The Swedish Meteorological and Hydrological Institute (SMHI) has measured waves at a few locations on the Swedish west coast, e.g. offshore of Väderöarna ($\sim$ 50 km NW of the test site). The observations are fragmented in time. However, a wave time series at Väderöarna covers 2005 March to present and is available on-line (http://opendata-catalog.smhi.se/explore/). Waves at the Islandsberg test site has been measured by Uppsala University since 2004 (Leijon et al., 2008). The observations, 2006 - present, of significant wave height are presented on-line (www.teknik.uu.se).

1.4 Aim of this report

This report describes the wave energy potential in the area covering, and surrounding, the Islandsberg test site.

To assess the wave energy resource at a specific site, wave models can be used to simulate wave propagation from regional to local scale. This approach has been acknowledged by Pitt (2009), and applied by e.g. Atan, Goggins, and Nash (2016) and Waters et al. (2009). A similar approach is applied here using the MIKE 21 Spectral Wave model, developed by DHI (DHI, 2016b). DHI is a company that develops and applies knowledge in modelling water environments (www.dhigroup.com).

The characterization of the wave energy at Islandsberg describes the distribution of wave energy in space and time, and with respect to wave parameters, such as wave periods and wave heights. It supplements the wave observations at the test site, made by Uppsala University, in that it estimates the wave energy potential in a larger area surrounding the test site. The modelled wave characterization also estimates wave directions, which is not measured by the on-site wave buoy. The Islandsberg specific set-up of the model gives the possibility to study the local wave climate before the wave measurements started.

The wave characterization described in this report is beneficial for developers, looking for the optimal conditions to test new marine technologies. It is also of interest for coastal management (in terms of e.g. erosion and marine ecosystems). Detailed wave characterizations, like this one, can be informative for designing marine structures, which are exposed to extreme waves produced by storms, and to the cumulative effect of waves in general.

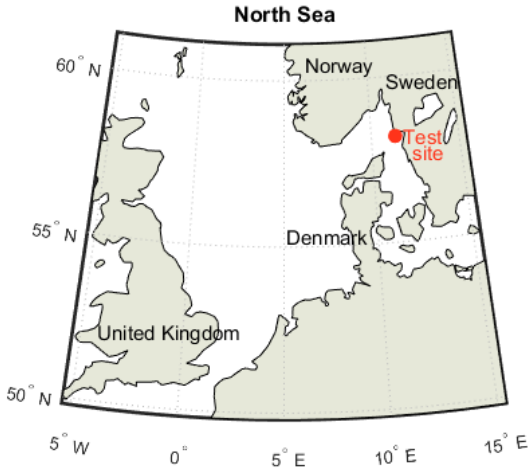

(a)

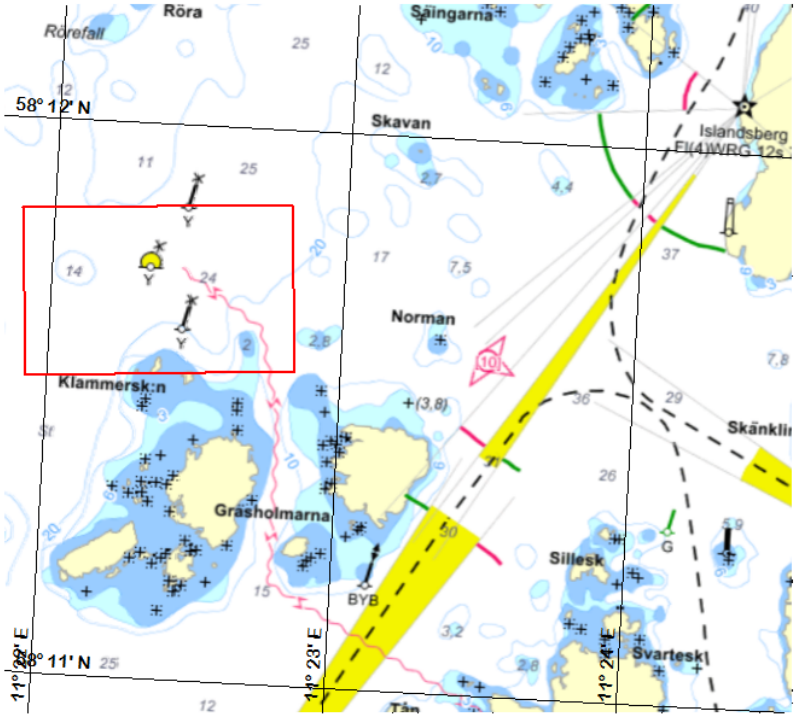

(b)

Figure 1: a) The location of the Islandsberg test site is indicated in red. An open ocean wind fetch extends southwestward from the test site to the North Sea. b) The test site area is marked (red line) on the sea chart offshore of Islandsberg. The test site coordinates were provided by Sundberg (2017). *Adapted from:* www.kartor.eniro.se

The impact of a modelled Wave Energy Converter (WEC), located at the test site, will be addressed as a supplementary aim of this study. Part of the wave energy is absorbed by the WEC, meaning that the WEC alters the propagating waves. The changes induced by the WEC to the local wave field is described in this report, beside the main focus of characterizing the wave potential at the Islandsberg test site.

1.5 A note on Wave Energy Converters

A variety of WEC systems have been invented during the last century, with different technical solutions to convert the kinetic and potential energy of waves into electricity (for an overview, see e.g. Callaway, 2007; de O. Falcão, 2010). Pilot WECs have also demonstrated the possibility to drive pumps from the dynamic pressure in waves for fresh water production (Williams, 2013). Fresh water can be produced by WEC-generated electricity in coastal communities. A desalination plant in Vizhinjam, India, was reported to produce 10 m^3 fresh water per day in 2005, powered by a battery bank that in turn was charged by WECs (Davies, 2005).

The different technical solutions of WEC systems can be categorized by three groups of working principles; 1) the oscillating body, 2) the overtopping device and 3) the oscillating water column (de O. Falcão, 2010). The three working principles will be briefly described below to give an introduction to WECs, with special emphasis on 1) which will be studied further. Schematic examples of the working principles are visualized in Fig.2.

1) The oscillating body system can be described by the WEC developed by the Division of Electricity at Uppsala University, visualized in Fig.2a. The WEC consists of a floating buoy, connected via a line to a translator that can move up and down in a stator, placed on the sea floor. Waves at the surface causes an oscillating movement that generates electricity. Research and development of the WEC has been conducted at the Islandsberg test site (e.g Leijon et al., 2008; Waters et al., 2011).

2) An overtopping WEC utilizes the vertical distance between the wave crests and the mean sea level. Waves spill water in the WEC container as they hit its sides. The collected water is then drained from the container through a turbine, generating electricity from the outflowing water. An example of an overtopping WEC can be seen in Fig. 2b.

3) The oscillating water column allows the wave motion to push air in a partly submerged tube. The air flow is forced through a turbine to produce electricity. An example of an oscillating column is visualized in Fig. 2c.

The WEC working principles described above are designed to extract energy from the oscillating sea surface. Knowledge of local wave characteristics, e.g. wave periods and wave heights, are important for planning locations for installment, for optimizing the energy absorption, for designing structures that survive in powerful sea states occuring at the intended site etc.

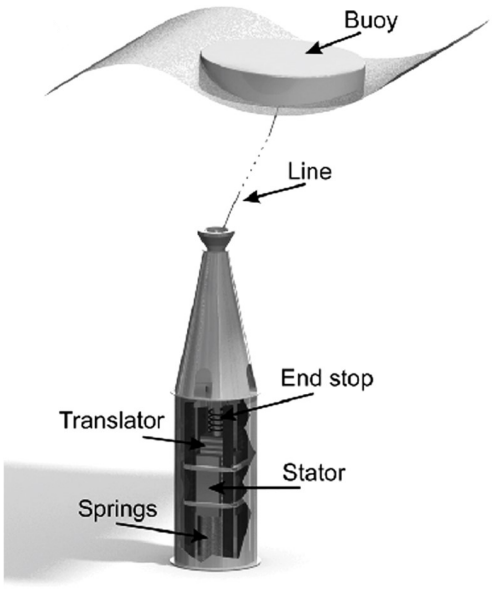

(a)

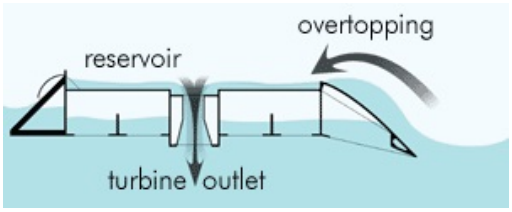

(b)

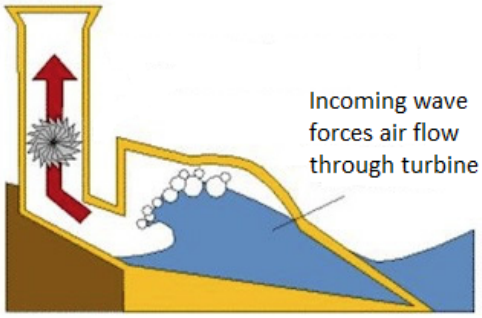

(c)

Figure 2: Schematics of three WEC systems; (a) Oscillating body WEC developed by Uppsala University. *Adapted from:* Engström, Eriksson, Goteman, Isberg, and Leijon, 2013. (b) Overtopping WEC developed by Wave Dragon. *From:* www.wavedragon.net. (c) Oscillating Water Column (OWC). *Adapted from:* www.es.travelbasquecountry.com/.

The Sotenäs wave power plant is located northwest of the Islandsberg test site and consists of a multi-generator park of WECs, the type described in 1) above (see Fig. 2a). The storm Urd during christmas 2016 caused 12 m high waves which snapped the wires to the WEC buoys at the Sotenäs power plant (Kristensson, 2017). Full-scale tests offshore can be helpful when evaluating the WEC design relative to some sea states, but extreme events at the intended site for installation also needs to be considered.

2 Method and materials

The MIKE 21 modelling system, the set-up of MIKE 21 SW for Islandsberg and the calibration and validation is described in the following sections.

2.1 MIKE 21 Flow Model FM

MIKE 21 Flow Model FM is a two-dimensional modelling system that numerically computes water motion with respect to wind and other forcing (DHI, 2016a). The system is based on a flexible mesh (FM), where the spatial domain is discretized into non-overlapping cells. MIKE 21 is a modular system.The two sections below describe the MIKE 21 Hydrodynamic Module and Spectral Wave Module that are applied in this study.

2.1.1 MIKE 21 Hydrodynamic Module

The computational base of the MIKE 21 Flow Model FM is the Hydrodynamic Module. It calculates the depth-averaged horizontal velocities and transport of salt and temperature with respect to forcing and boundary conditions.

The water level and flow velocity are computed by solving the two-dimensional shallow water equations, i.e. the depth-integrated incompressible Reynolds averaged Navier-Stokes equations (DHI, 2016a). For an introduction to the two-dimensional shallow water equations see, for example, Kundu and Cohen (2004).

2.1.2 MIKE 21 Spectral Wave Module

The Spectral Wave module MIKE 21 SW simulates the evolution, transformation and decay of wind-generated surface waves and swell (DHI, 2016b). MIKE 21 SW includes wave-growth by momentum transfer from the wind. Coastal wave phenomena such as refraction and shoaling are accounted for and the dissipation functions include depth-induced wave breaking, white capping, bottom friction etc.

MIKE 21 SW computes the directional-frequency wave action spectrum, N, for each instance in time and space. An adaptive time step is applied, so that the local increment in time is restricted by the CFL condition $C < 1$, where C is the Courant number. MIKE 21 SW is coupled with the Hydrodynamic Module in terms of the time-varying water level.

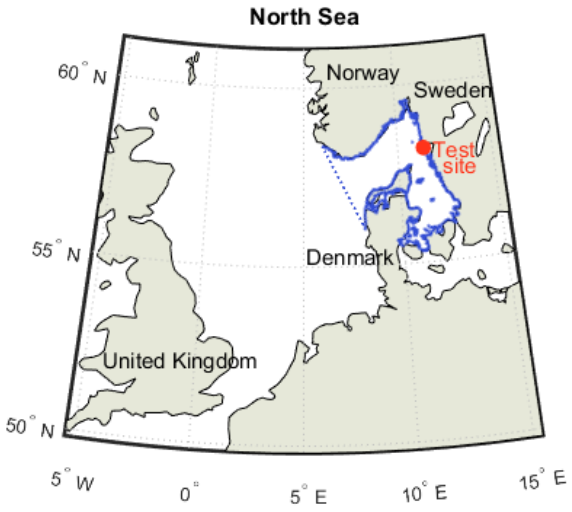

Figure 3: The model domain covering Skagerrak and Kattegat is outlined in blue. The western domain boundary (dotted blue line) is open to the North Sea.

The conservation equation for wave action can be written as

$$\frac{\delta N}{\delta t} + \nabla \cdot (\vec{v}N) = \frac{S}{\sigma} \tag{1}$$

where $N = N(\vec{x}, \sigma, \theta, t)$ is the action density, $\vec{x} = (x, y)$ are Cartesian coordinates, σ is the relative angular frequency, θ is the wave direction and t is the time. The wave action density is related to the energy density spectrum, E, by $N = E/\sigma$. The propagation of the wave group in $(\vec{x}, \sigma, \theta)$ space is represented by $\vec{v}$ in Eq. 1. S represents the source terms (describing wind input), sinks (due to whitecapping, bottom friction and depth-induced wave breaking) and a term for non-linear wave-wave interaction in the energy balance. Details on the computations of the sea states can be found in DHI (2016b) and Komen et al. (1994).

2.2 The Islandsberg set-up of MIKE 21 SW

To characterize the local wave energy potential at the Islandsberg test site, a model was set up covering Skagerrak and Kattegat with an open boundary to the North Sea (see Fig. 3). The model is forced by wind. Regional wave and water level data was applied as input at the open North Sea boundary. The process of setting up the model is described below.

2.2.1 Bathymetry

The regional bathymetry data used for Kattegat and Skagerrak was extracted from EMODnet Bathymetry (see www.emodnet.eu for details).

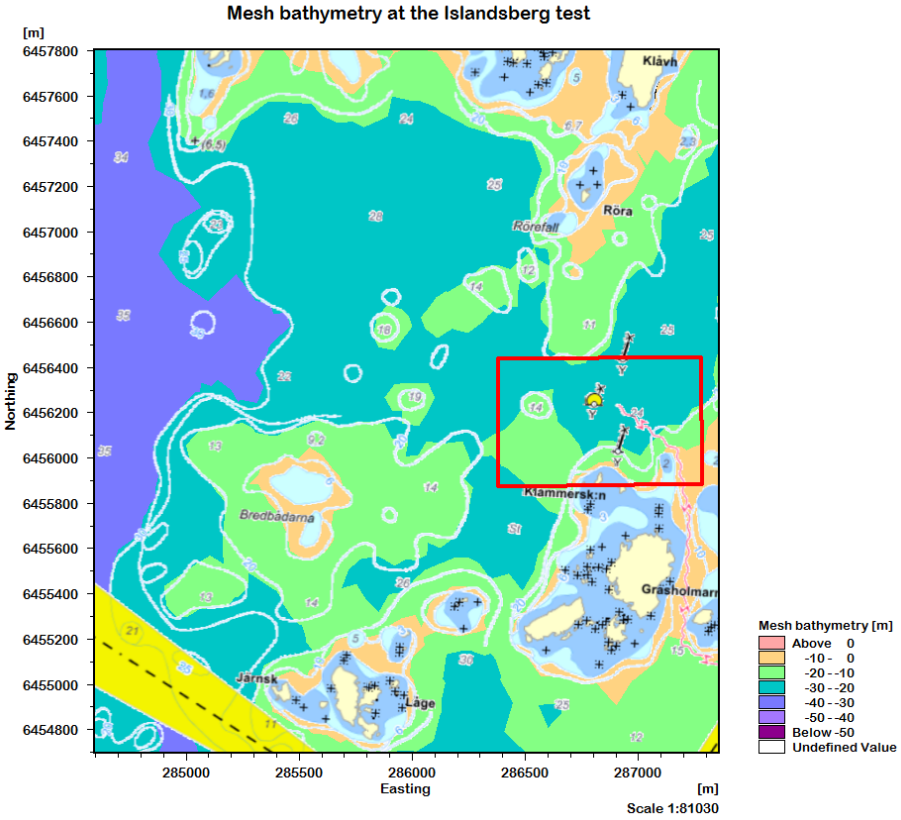

Figure 4: The mesh bathymetry is visualized (color scale) at the Islandsberg test site (red). The sea chart items (islands, depth contours, depths in numbers etc.) are from www.kartor.eniro.se.

Local bathymetry surrounding the testsite was provided from MIKE C-MAP, based on C-MAP digital charts. For more information on MIKE C-MAP, see www.mikepoweredbydhi.com.

For a visual comparison of the generated mesh bathymetry and sea chart depths near the test site, see Fig. 4. The bathymetry data was integrated to give the depth at each grid cell, see Fig. 5.

2.2.2 Mesh and resolution

The spatial grid visualized in Fig. 5 is a flexible mesh, with increasing resolution towards coastlines and, in particular, towards the test site (see Fig. 5b). The side length of each grid cell in the finest resolved area surrounding the test site is ~ 100 m. This is a typical scale of resolution when modelling waves in coastal waters according to (Holthuijsen, 2007).

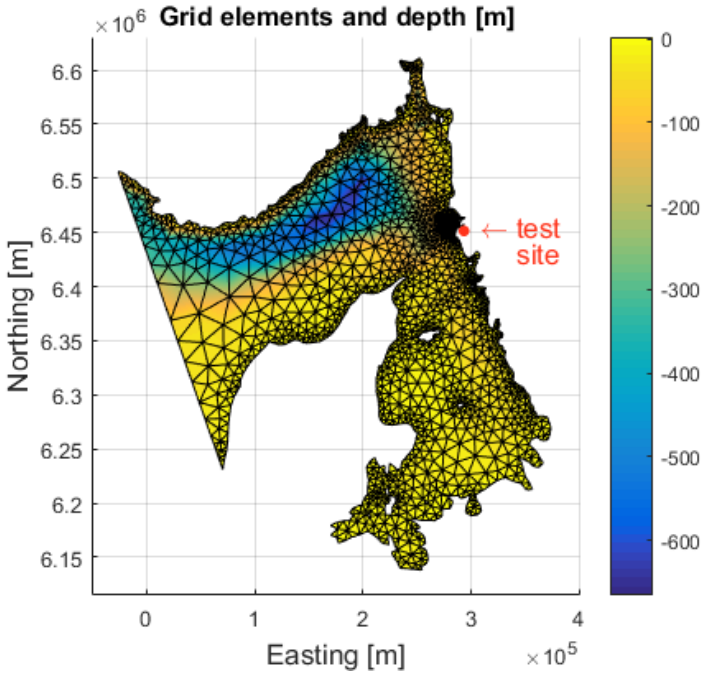

(a)

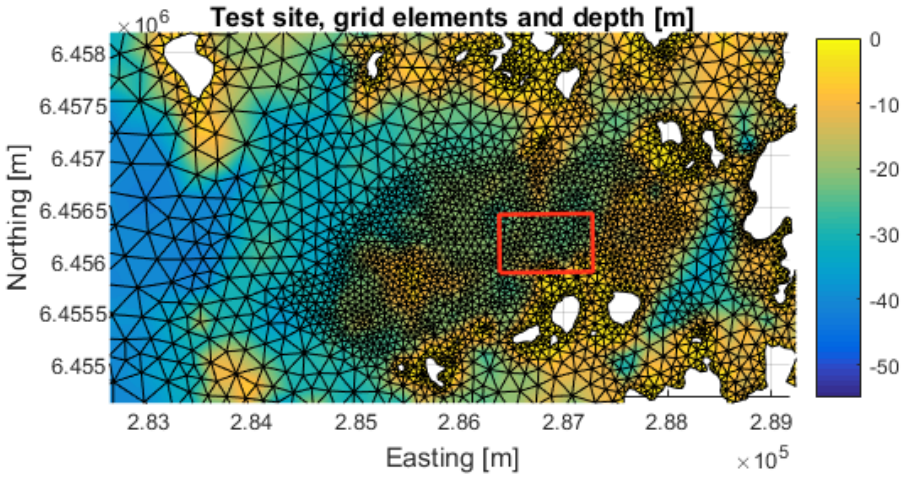

(b)

Figure 5: a) The model grid elements (black) are visualized, with depth indicated in color. The resolution of the grid increases towards the test site. b) Grid elements (black) and depth (color scale) are visualized nearby the test site area (red).

The process of generating and optimizing the mesh is time consuming, but necessary for the model to run in a reasonable amount of time and to produce results with desired accuracy. Multiple attempts were made and the mesh with the best level of performance was chosen. The bathymetry data was interpolated for the generated grid elements (see previous section, Fig. 4 and 5).

The spectral resolution was evaluated for a simulated test period of 14 days, in February 2008, where model results were compared with observations from the test site. The evaluation resulted in a spectral resolution of 24 directions ($\Delta\theta = 15^o$) and 25 discrete frequencies, f_n, distributed in the interval $[0.05, 0.76]$ Hz (corresponding to wave periods $T \in [1.3, 20]$ s). The distribution of discrete frequencies was specified as $f_n = f_0 c^{n-1}$ (where $f_0 = 0.05$ is the minimum frequency, $c = 1.12$ is the frequency factor, and $n = 1, 2, ..., 25$). The resolution of the frequencies is increasing towards the lower frequency part of the spectrum (corresponding to longer wave periods). The comparison between simulations and observations is further explained in 2.3.

2.2.3 Forcing

An accurate representation of wind conditions is of great importance when modelling surface waves. In fully developed sea the significant wave height is proportional to the square of the wind speed, meaning that wind generated waves are sensitive to variations in the wind input (Komen et al., 1994).

The wind forcing applied originates from the Climate Forecast System Reanalysis (CFSR) data set, established by the National Centers for Environmental Prediction (NCEP). The CFSR data set was established from satellite measurements to represent globally gridded atmospheric states from 1979 to present. The temporal resolution of the CFSR data is 1 hour, and the spatial resolution is 0.5^o x 0.5^o. For more details on CFSR, see Saha et al., 2010. The CFSR data parameters applied in this study are wind magnitude and direction. The wind data for 2005 is visualized in Fig. 6 for comparison with wind observations at the SMHI wind measuring station Väderöarna ($\sim$ 50 km northwest of the test site). The SMHI observed wind magnitude in Fig. 6 has been converted to wind magnitude at 10 m above mean sea level, following the method of Smith, 1988. SMHI wind observations at Väderöarna and Måseskär ($\sim$ 10 km S of the test site) are visualized in Fig. 7.

Sea level variations and wave spectra at the domain boundary inlet from the North Sea was extracted from a DHI hindcast database.

2.3 Calibration and validation

Several test runs of the model were evaluated in terms of different settings of dissipation parameters. The model was calibrated in this way, comparing the results with wave observations at the test site. The settings giving the estimations closest to observed values was then applied for a validation run to confirm that the model is well calibrated to the local conditions at Islandsberg.

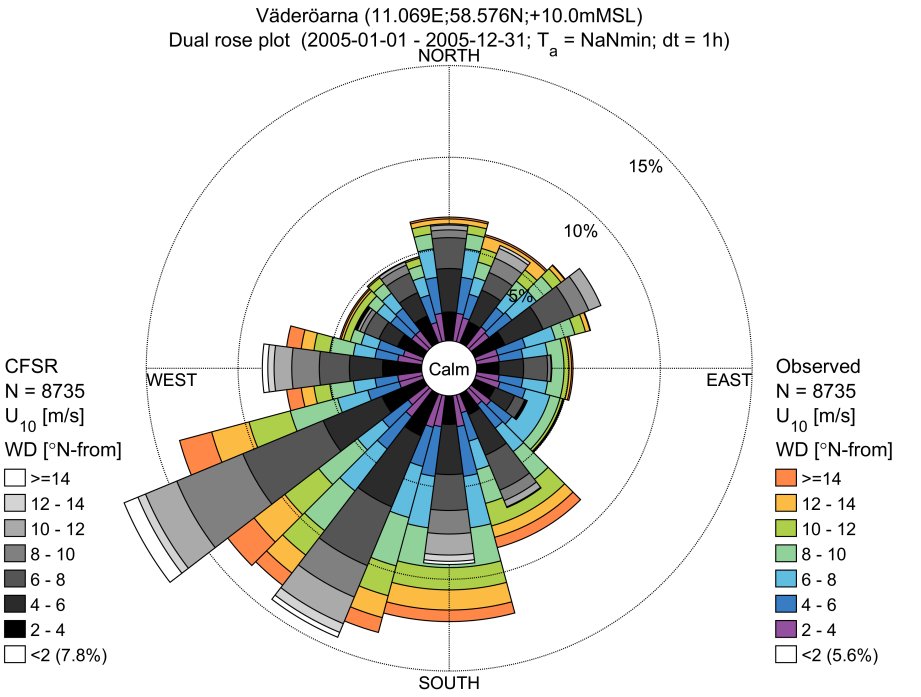

Figure 6: Wind speed and directions in 2005 are visualized at Väderöarna. The wind magnitude at 10 m above MSL, U_{10}, and wind direction, WD, originates from CFSR data (grey) and SMHI observations (color).

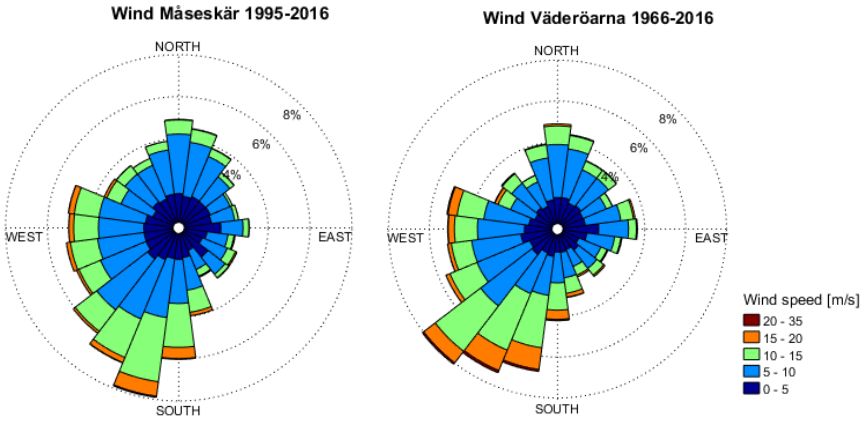

Figure 7: Wind measured by SMHI at Måseskär, south of Islandsberg, and at Väderöarna, north of Islandsberg, on the Swedish west coast.

Waves have been observed at the Islandsberg test site by a Datawell Waverider^{TM} buoy, courtesy of Uppsala University. The buoy measures the surface elevation at its position, at a sampling frequency of 2.56 Hz. Raw data from the buoy was provided for years 2008 and 2009 by Uppsala University. The data was processed to give spectral wave parameters for every half hour describing the sea state during that time. Spectral wave parameters are defined from the power frequency spectrum $S_{power}(f)$, where f is the discrete frequency in this case, as e.g. the significant wave height,

$$H_{m0} = 4\sqrt{m_0} \tag{2}$$

the mean wave period,

$$T_{01} = \frac{m_0}{m_1} \tag{3}$$

and the energy period

$$T_{-10} = \frac{m_{-1}}{m_0} \tag{4}$$

where $m_n = \int_0^\infty f^n S_{power}(f) df$ (e.g Komen et al., 1994; Tucker and Pitt, 2001). The power spectrum representation, $S_{power}(f)$, of the elevation time series observed at Islandsberg was computed using the Fast Fourier Transform function in Matlab, according to recommendations from Engström, 2017. The conversion of discrete ocean wave records to power spectra via Fourier transform is described in e.g. Tucker and Pitt (2001) and Holthuijsen (2007).

Comparing observed and modelled wave time series was done by calculations of the scatter index

$$SI = \frac{\sqrt{\frac{1}{N}\sum_{i=1}^{N}(obs - mod - bias)_i^2}}{\overline{obs}} \tag{5}$$

and correlation coefficient

$$CC = \frac{\sum_{i=1}^{N}(obs_i - \overline{obs})(mod_i - \overline{mod})}{\sqrt{\sum_{i=1}^{N}(obs_i - \overline{obs})^2 \sum_{i=1}^{N}(mod_i - \overline{mod})^2}} \tag{6}$$

where *obs* are observations, *mod* are modelled values, and *bias* is the mean of the difference; $bias = \frac{1}{N}\sum_{i=1}^{N}(obs - mod)_i$.

Comparing SI and CC for several runs, varying one model parameter at a time, gave the model set-up with the best fit between modelled and observed data. The model parameters scaling the source function that simulates dissipation due to whitecapping were identified to be of importance for accurately simulating the waves at Islandsberg. Several values of those parameters, c_{dis} and δ_{dis}, were tested to find the best combination. A table of tested model parameters is given in Appendix A.

The significant wave height is important for the wave energy and hence was considered in the calibration process. The deep water energy flux approximation gives

$$E = \frac{\rho g^2}{64\pi} T_{-10} H_{m0}^2 \tag{7}$$

where ρ is the sea water density, g is the acceleration of gravity and the energy flux, E, is dependent on the significant wave height to second order (Tucker and Pitt, 2001).

The final time series comparison of observed and simulated significant wave height is visualized in Fig. 8. The period used in the calibration process is shown in Fig. 8a and a longer validation period was examined for confirmation of the applied settings (see Fig. 8b).

The statistical comparison measures of the validation period of significant wave height (Fig. 8b) are $SI = 0.17$ and $CC = 0.98$.

The wave period also affect the energy flux in Eq. 7, and it is important for optimizing the WEC resonance frequency. The mean wave period, T_{01}, was chosen for calibration purposes since it is less sensitive to high frequency noise than spectral wave periods of higher moments (Holthuijsen, 2007). The statistical comparison of modelled and observed T_{01} for the validation period gave $SI = 0.15$ and $CC = 0.80$. The aim was to calibrate the model so that low SI values and high CC values were obtained for both wave heights and wave periods. The results of the calibration and validation were satisfactory in that the applied model settings simulates waves close to observations. The applied model settings, resulting from the calibration, are summarized in Appendix A. Wave diffraction was not included in the model set-up.

2.4 The WEC test

For studying the effect of a WEC at the test site a local test case was performed. The result of the modelled waves during January 2005 in the area surrounding the test site was applied to this smaller case. The case included two runs, one including a WEC at the center of the test site and one excluding the WEC. The case was performed so that the effect on mean wave power could be evaluated by comparing the two runs. The simulated period was three weeks. Wind forcing was not included in this case. The WEC itself was defined by a capture width setup representing a point absorbing WEC, the type described by 1) in 1.5, with a buoy diameter of 4 m. The capture width, $CW = P/J$ where P is absorbed power (in kW) and J is wave energy resource (in kW/m), is compared for different WECs by Babarit (2015). This setup models the WEC as a local wave energy sink at its position in the mesh. The WEC was placed in the centre of the test site at 58.20°N, 11.37°E.

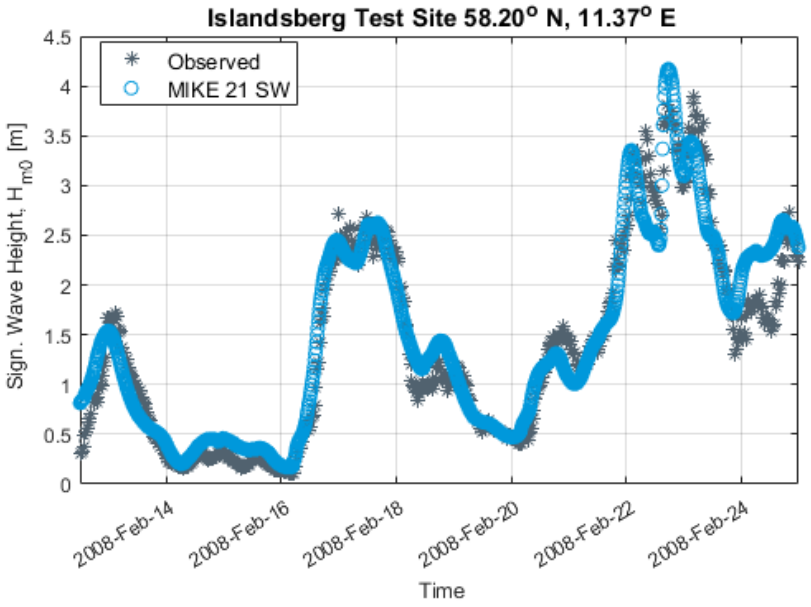

(a)

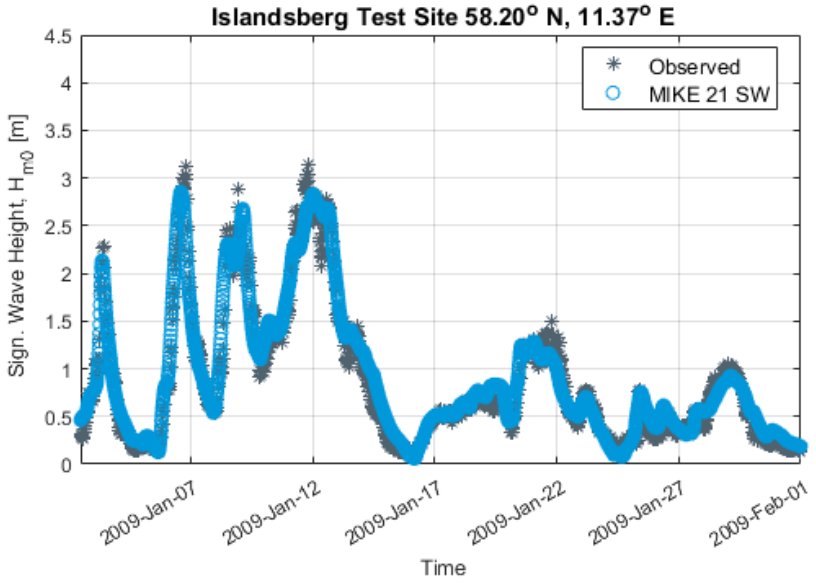

(b)

Figure 8: The time series of modelled and observed significant wave height at the Islandsberg test site are visualized during a) two weeks chosen for calibration against the observed values, b) one month for the validation of the model.

3 Results

The modelled wave characteristics covering the years 2005-2009 are described below. The results in 3.1 refer to the local area including and surrounding the test site. A more detailed description of distribution of sea states in terms of wave directions, energy periods and significant wave heights, is given for 58.20°N, 11.37°E in 3.2.

3.1 Local wave characteristics

The spatial and temporal distribution of the local wave characteristics, surrounding Islandsberg, are presented in this section.

The mean wave energy flux is visualized in Fig. 9. The mean is taken over the winter season (October-March) in Fig. 9a, and over the summer (April-September) in Fig. 9b. There is a general difference in higher mean wave power in the winter than in the summer season in the area at, and offshore of, the test site (visualized in grey). The mean wave power differs between the two seasons by ~ 3 kW/m at the test site (see Sec. 3.2). The spatial gradient in mean wave power (in the East-West direction) is larger in the higher energetic winter sea states (Fig. 9a) compared to the summer (Fig. 9b).

The mean wave power is seen to increase in the offshore direction to the west, where depth increases. A hot spot appears in the winter mean wave power (Fig. 9a) at (x,y) = (284000, 6455000), SW of the test site. The position is that of the shallows Skrämja and Skrämjas ungar, with rocks of less than 10 m depth.

A shadowing effect of the islands can be seen in Fig. 9, in that the mean wave power is lower to the east of the islands. It should be noted that wave diffraction was not included in the model.

The exceedance of $H_{m0} > 1$ m is visualized in Fig. 10 as fraction of time. The cumulative wave energy at the test site has previously been observed to be contributed by sea states with $H_{m0} \in [1.2, 2.7]$ m, based on one year of observations (Leijon et al., 2008). Therefore, the exceedance level of 1 m was chosen in Fig. 10.

The significant wave height at the position of the SMHI wave measurement buoy offshore of Väderöarna (58.48°N, 10.93°E), was compared in terms of simulations and observations in 2007. The correlation coefficient between the estimated and observed H_{m0} in 2007 was $CC = 0.95$. The scatter index was $SI = 0.26$.

The point 58.20°N, 11.37°E, located in the centre of the test site area, is marked in grey in Fig. 9 and 10. The modelled wave characteristics at this point will be further described in the following section.

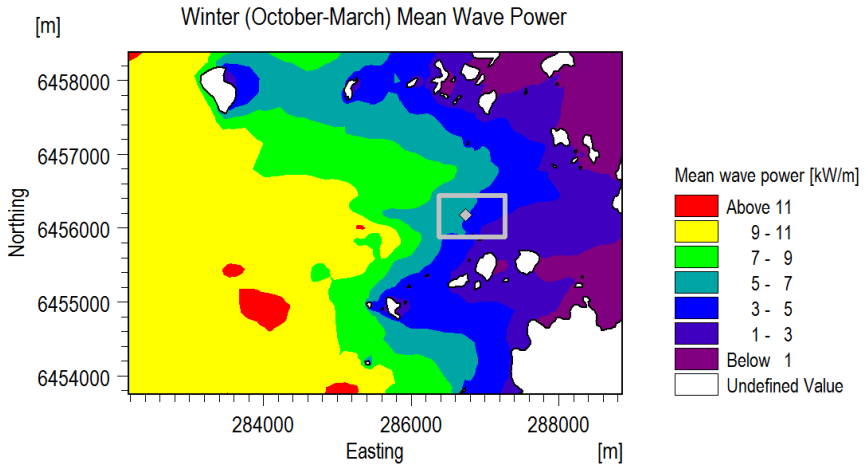

(a)

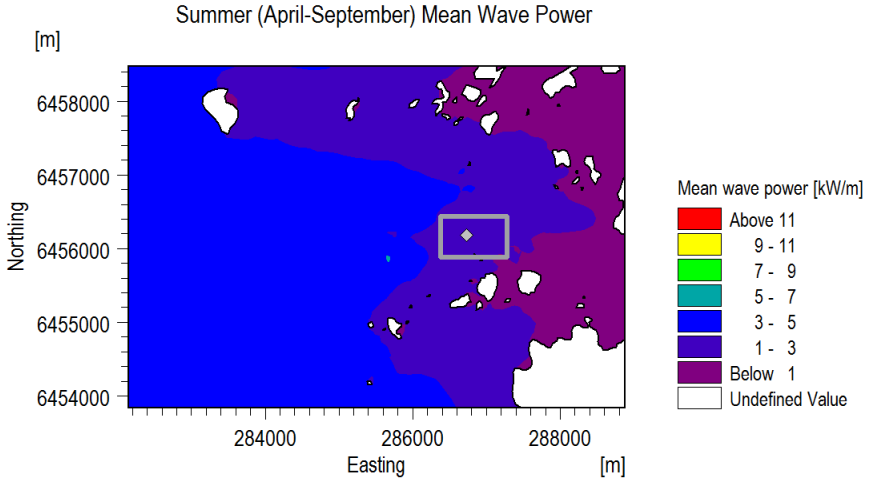

(b)

Figure 9: The seasonal mean of wave power (color scale) in the surroundings of the test site (grey) are visualized for a) the winter season (October-March) and for b) the summer (April-September).

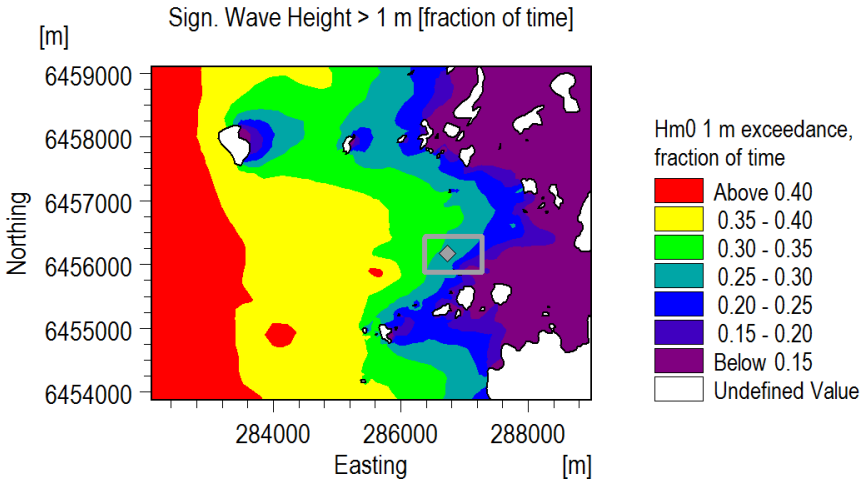

Figure 10: The fraction of time of significant wave height exceeding 1 m is visualized (color scale) at the test site (grey) and its surroundings.

3.2 Test site wave characteristics

Modelled wave parameters at $58.20^o N$,$11.37^o E$ *are described in this section. The geographical point was chosen since it is close to the position of the wave measurement buoy on-site.*

The estimations of mean wave direction and significant wave height are visualized in Fig. 11. The main part of the waves are seen to come from the west and west-southwest. The contribution of $H_{m0} > 2$ m is only seen arriving from the main westerly directions.

The frequency of occurence of sea states, represented by the distribution of wave energy period, T_{-10}, and significant wave height, H_{m0}, is visualized in Fig. 12. The energy period is divided in 0.5 s intervals, and the significant wave height in intervals of 0.25 m. The most frequent sea states are seen in the interval $T_{-10} \in [2, 6]$ s and $H_{m0} \in [0, 1.5]$ m. A few occurences of $H_{m0} > 5$ m are seen in Fig. 12. The highest maximum wave height during the storm Gudrun was estimated to 9.9 m.

The mean annual energy flux corresponding to each sea state is visualized in Fig. 13. The axis intervals are the same as in Fig. 12. The mean cumulative energy contribution at this site is seen to be represented by sea states of about $T_{-10} \in [5, 8]$ s and $H_{m0} \in [1, 3]$ m.

The modelled mean wave power at this position is 3.7 kW/m. The corresponding summer mean (April-September) is 2.4 kW/m, and the winter mean (October-March) is 5.1 kW/m.

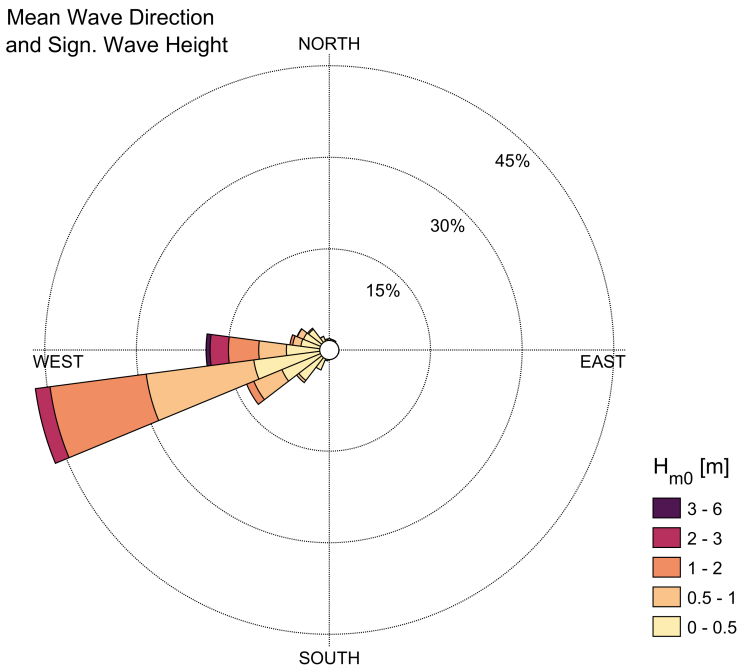

Figure 11: The significant wave height, H_{m0}, and mean wave direction at the test site (58.20^{o}N,11.37^{o}E).

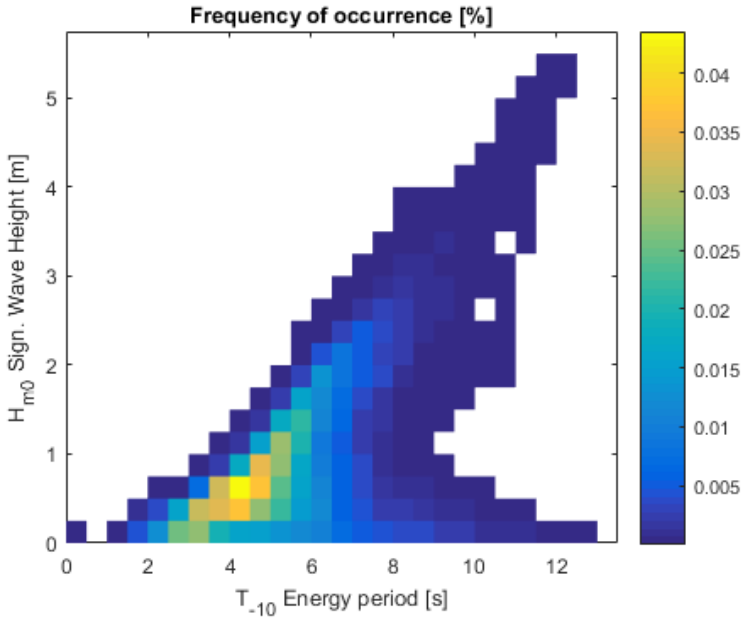

Figure 12: The occurrence of sea states are visualized as occurrence of wave energy period and significant wave heights (in % of the 5 years of modelled data).

3.3 The WEC test

The test case with a point absorbing WEC included in the centre of the Islandsberg test site area is visualized in Fig. 14. The mean wave power of the model including the WEC is visualized relative to a reference model run excluding the WEC. Fig. 14 shows a local decrease in mean wave power extending $\sim$ 500 m east of the WEC position. Up to 6% of the wave energy is absorbed in the closest vicinity of the WEC. At a $\sim$ 500 m distance away from the WEC, the difference in mean wave power due to the WEC is only a few percent.

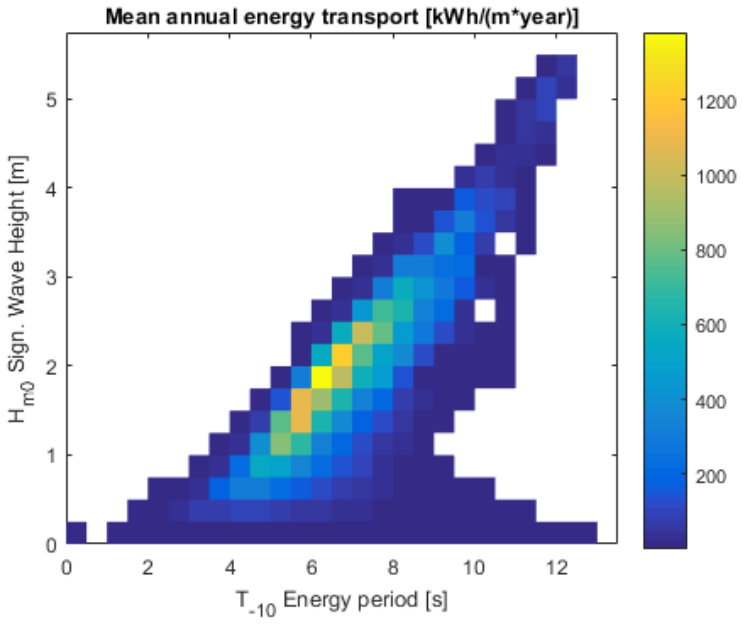

Figure 13: The mean annual energy transport, based on the five years of modelled wave data, is visualized (color) at corresponding sea states of T_{-10} and H_{m0}.

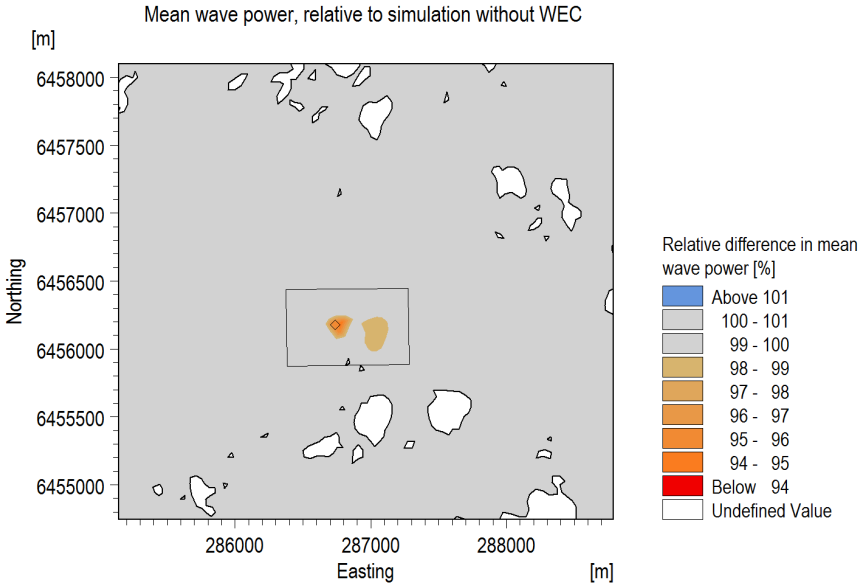

Figure 14: The mean wave power of the test case including a WEC is visualized (color) relative to the model result without the WEC. The WEC position and the test site area are outlined in black.

4 Summary and discussion

The mean wave power 3.7 kW/m (based on the 2005-2009 simulations), at 58.20^oN,11.37^oE, is close to the observed 3.4 kW/m mean wave power (based on measurements in 2007) by Leijon et al. (2008). Both values are higher than the mean wave power estimate 2.6 ± 0.3 kW/m, based on modelled data covering the years 1997-2004 (Waters et al., 2009). The higher mean wave power estimate obtained here could partly be explained by different time coverage. The estimate of Waters et al. (2009) is however close to the summer mean wave power of 2.4 kW/m at the test site.

The winters in the present model covered the storms Gudrun (January, 2005) and Per (January, 2007) which contributed to the higher winter mean wave power of 5.1 kW/m at the test site. The winter season generally contains stronger winds, and was therefore expected to contain more energetic sea states.

Other than Gudrun and Per, the modelled period in this study cover the summer storms in 2008. The year 2009, which was classified as a storm free year by SMHI, was also included. Although covering a range of different weather conditions, the 5 years of established wave data is somewhat short compared to similar studies (e.g. Atan et al., 2016; Waters et al., 2009). However, it is valuable to establish accurate estimations rather than aiming for fast calculations and long time coverage.

The significant seasonal difference between winter and summer mean wave power shown here (Fig. 9) has likewise been estimated for offshore Skagerrak by Waters et al. (2009).

The good correlation between modelled values and observations (see Fig. 8) suggests that the forcing and settings applied in this model are representative for the wave conditions at the on-site wave buoy position. It also suggests that the propagation of model wave energy through the domain is representative for the Skagerrak and Kattegat. It is hard however to say if the simulations in the area surrounding the buoy position is as accurate. However, the comparison check of the 2007 simulations of H_{m0} with the SMHI observations at Väderöarna gave satisfactory results. Meaning that the model shows capacity of estimating the prevailing wave conditions also at a distance from the highest resolved area for which the model was calibrated. Caution should be applied when interpreting results at the eastern coasts of the islands surrounding the test site, since diffraction has not been included.

It is interesting to note that the result of the calibration of the Islandsberg model set-up, is similar to that of Atan et al. (2016), where the whitecapping dissipation was found to be important to characterize the wave energy at the Atlantic Marine Energy Test Site (AMEST), at the Irish west coast. The AMEST and Islandsberg models share the basic approach, i.e. numerical wave propagation from regional to local scale.

The winter mean wave power hot spot at the shallow Skrämja (Fig. 9a) is noticeable in the $H_{m0} > 1$ exceedance (Fig. 10). The wave power hot spot is therefore likely caused by shoaling, which increases the wave amplitude at shallow areas before breaking. However, dissipation due to depth-induced wave

breaking and bottom friction gives a general reduction of wave heights (and wave power) in the direction of decreasing depths towards the coast (Fig. 9 and 10).

The exceedance of significant wave heights in Fig. 10 are of interest for the accessibility of the site in terms of diving and maintenance operations.

An interesting result is the larger spatial variation in the energetic sea states in the winter than in the summer (compare Fig. 9a with 9b). This suggests that a detailed spatial resolution is preferred when evaluating the wave energy potential at areas of interest for e.g. installing WECs. The exceedance of H_{m0} in Fig. 10 also show considerable spatial variation in the test site area. Energetic sea states are more frequently available west of the test site at greater depth.

The mean wave direction in Fig. 11 shows a dominating direction coming from the west-southwest. This was expected due to the dominating winds from west-southwest (Fig. 6 and 7). Similar wave directional conditions were also published by Waters et al., 2009. The highest waves in Fig. 11 also come from the west-southwest due to the long wind fetch in that direction.

The significant wave heights at the centre position of the test site is reaching up to 5.5 m (see Fig. 12). Again, this is higher than the result in Waters et al., 2009, probably due to the different modelled time periods (where 2005-2009 include the storms Gudrun and Per). The on-line time series of H_{m0} observed at the test site show several occurrences of significant wave heights $\sim$ 5 m, for example during the storm Gorm (December, 2015) and Urd (December, 2016).

The sea states and cumulative energy transport in Fig. 12 and 13 much resembles the distribution of wave energy in time and with respect to energy period and H_{m0} as was described by the 2007 observations in Leijon et al., 2008.

Sea level observations reached almost 1.5 m above mean sea level in Kattegat and Skagerrak during the storm Urd (SMHI, 2016). Storm surges allows powerful sea states to propagate closer to the coast, due to less depth-induced wave breaking.

The highest maximum wave height simulated during the storm Gudrun was 9.9 m. The value is larger than the statistical highest 100 year wave estimated to 6.2 m by Waters et al., 2009 (which did not include Gudrun). The estimation of maximum wave heights (assuming Rayleigh distributed wave heights) can give somewhat large values in coastal waters, but a general rule for storms is $H_{max} \approx 2H_{m0}$ (Holthuijsen, 2007). The model estimate of the 9.9 m high wave during Gudrun therefore match well with the observed significant wave heights of $\sim$ 5 m during storms (such as Gorm and Urd) at Islandsberg (see on-line timeseries, www.teknik.uu.se). Moreover, a 9 m high wave has been confirmed to be observed at the test site (Engström, 2017).

The impact of a single WEC on the mean wave power was evaluated by the set-up of a smaller model. The experiment showed a mild decline of mean wave power reaching $\sim$ 500 m to the east of the WEC. This experiment should be interpreted as an introductory example. Devices with higher capture widths would reduce the surrounding mean wave power further, in this model set-up. Moreover, it doesn't account for the WEC-wave interaction that would produce e.g. radiating waves. A model resolving these effects can give more

understanding of WEC effect on the surrounding wave climate.

5 Conclusion

The simulated period 2005-2009 covered rough wave events such as a 9.9 m high wave, during the storm Gudrun, in the centre of the Islandsberg test site. The high spatial resolution in the local area surrounding the test site was able to resolve large spatial variability in the coastal wave power potential. The spatial resolution is noted to be important when planning offshore installation sites.

6 Acknowledgements

Many thanks goes to Christin Eriksson (DHI) and Anne Gunnäs (Lysekils kommun) for initiating this master thesis project. I am most grateful for contributions and interest shown by Kerstin Hindrum and RISE. The supervision and advice from Martin Johnsson (DHI), Torsten Linders (University of Gothenburg) and Jens Engström (Uppsala University) has been of great value throughout the project. I would also like to thank Mats Leijon, Jan Sundberg and Rafael Waters (Division of Electricity, Uppsala University), for providing expertise and data. Björn Elsäßer (School of Natural and Built Environment, Queen's University Belfast, and DHI Denmark) provided suggestions and explanations of modelling a WEC, for which I am very grateful.

References

Atan, R., Goggins, J., & Nash, S. (2016). A Detailed Assessment of the Wave Energy Resource at the Atlantic Marine Energy Test Site. *Energies*, *9*. doi:10.3390/en9110967

Babarit, A. (2015). A database of capture width ratio of wave energy converters. *Renewable Energy*, *80*, 610–628. doi:http://dx.doi.org/10.1016/j.renene.2015.02.049

Callaway, E. (2007). To catch a wave. *Nature*, *450*, 156–159.

Cato, I. & Kjellin, B. (2008). Maringeologiska undersökningar vid vågkraftsanläggning utanför Islandsberg, Bohuslän. *Sveriges geologiska undersökning, SGU-rapport 2008:10*.

Clément, A., McCullen, P., Falcão, A., Fiorentino, A., Gardner, F., Hammarlund, K., ... Thorpe, T. (2002). Wave energy in Europe: current status and perspectives. *Renewable and Sustainable Energy Reviews*, *6*(5), 405–431. doi:http://dx.doi.org/10.1016/S1364-0321(02)00009-6

Davies, P. (2005). Wave-powered desalination: resource assessment and review of technology. *Desalination*, *186*(1), 97–109. doi:http://dx.doi.org/10.1016/j.desal.2005.03.093

de O. Falcão, A. F. (2010). Wave energy utilization: A review of the technologies. *Renewable and Sustainable Energy Reviews*, *14*(3), 899–918. doi:http://dx.doi.org/10.1016/j.rser.2009.11.003

DHI. (2016a). *MIKE 21 & MIKE 3 Flow Model FM, Hydrodynamic and Transport Module, Scientific Documentation*. DHI. Hørsholm.

DHI. (2016b). *MIKE 21, Spectral Wave Module, Scientific Documentation*. DHI. Hørsholm.

Energimyndigheten. (2016, November). El-, gas- och fjärrvärmeförsörjningen 2015. Retrieved from http://www.scb.se/Statistik/EN/EN0105/2015A01/EN0105_2015A01_SM_EN11SM1601.pdf

Engström, J. (2017). Division of Electricity, Uppsala University. Personal communication.

Engström, J., Eriksson, M., Goteman, M., Isberg, J., & Leijon, M. (2013). Performance of large arrays of point absorbing direct-driven wave energy converters. *Journal of Applied Physics*, *114*. doi:10.1063/1.4833241

Falnes, J. (2007). A review of wave-energy extraction. *Marine Structures*, *20*(4), 185–201. doi:http://dx.doi.org/10.1016/j.marstruc.2007.09.001

Holthuijsen, L. (2007). *Waves in Oceanic and Coastal Waters*. Cambridge University Press, New York.

Komen, G., Cavaleri, L., Doneland, M., Hasselmann, K., Hasselmann, S., & Janssen, P. (1994). *Dynamics and Modelling of Ocean Waves*. Cambridge University Press.

Kristensson, J. (2017, March). "Jag tror inte att Seabased fullföljer projektet". *Ny Teknik*. Retrieved from http://www.nyteknik.se/energi/jag-tror-inte-att-seabased-fullfoljer-projektet-6830164

Kundu, P. & Cohen, I. (2004). *Fluid mechanics* (3rd ed.). Elsevier Academic.

Langhamer, O. (2010). Effects of wave energy converters on the surrounding soft-bottom macrofauna (west coast of sweden). *Marine Environmental Research*, *69*(5), 374–381. doi:https://doi.org/10.1016/j.marenvres.2010.01.002

Leijon, M., Boström, C., Danielsson, O., Gustafsson, S., Haikonen, K., Langhamer, O., ... Waters, R. (2008). Wave Energy from the North Sea: Experiences from the Lysekil Research Site. *Surveys in Geophysics*, *29*(3), 221–240. doi:10.1007/s10712-008-9047-x

Ocean Energy Europe. (2017, March). MaRINET2. Retrieved from https://www.oceanenergy-europe.eu/en/eu-projects/current-projects/marinet2

Pelc, R. & Fujita, R. M. (2002). Renewable energy from the ocean. *Marine Policy*, *26*(6), 471–479. doi:http://dx.doi.org/10.1016/S0308-597X(02)00045-3

Pitt, E. [Edward]. (2009). *Assessment of Wave Energy Resource*. European Marine Energy Centre Ltd (EMEC). BSI, 389 Chiswick High Road, London W4 4AL.

Rogner, H.-H., Aguilera, R. F., Archer, C., Bertani, R., Bhattacharya, S. C., Dusseault, M. B., ... Yakushev, V. (2012). Chapter 7 - Energy Resources and Potentials. In *Global Energy Assessment - Toward a Sustainable Future* (pp. 423–512). Cambridge University Press, Cambridge, UK, New

York, NY, USA, and the International Institute for Applied Systems Analysis, Laxenburg, Austria.

Saha, S., Moorthi, S., Pan, H.-L., Wu, X., Wang, J., Nadiga, S., ... Goldberg, M. (2010). The NCEP Climate Forecast System Reanalysis. *Bulletin of the American Meteorological Society*, *91*(8), 1015–1057. doi:10.1175/2010BAMS3001.1

SMHI. (2016, December). Sammanfattning av stormen Urd. Retrieved from https://www.smhi.se/nyhetsarkiv/sammanfattning-av-stormen-urd-1.113390

Smith, S. D. (1988). Coefficients for sea surface wind stress, heat flux, and wind profiles as a function of wind speed and temperature. *J. Geophys. Res. 93*. doi:10.1029/JC093iC12p15467

Sundberg, J. (2017). Division of Electricity, Uppsala University. Personal communication.

Tucker, M. & Pitt, E. [E.G.]. (2001). *Waves in Ocean Engineering*. Elsevier Ocean Engineering Book Series. The Boulevard, Langford Lane, Kidlington, Oxford OX5 1GB, UK: Elsevier Science Ltd.

Waters, R., Engström, J., Isberg, J., & Leijon, M. (2009). Wave climate off the Swedish west coast. *Renewable Energy*, *34*(6), 1600–1606. doi:http://dx.doi.org/10.1016/j.renene.2008.11.016

Waters, R., Rahm, M., Eriksson, M., Svensson, O., Strömstedt, E., Boström, C., ... Leijon, M. (2011). Ocean wave energy absorption in response to wave period and amplitude : offshore experiments on a wave energy converter. *IET Renewable Power Generation*, *5*(6), 465–469.

Williams, A. (2013). "Wave-powered Desalination Riding High in Australia". *WWi magazine*. Retrieved from http://www.waterworld.com/articles/wwi/print/volume-28/issue-6/regional-spotlight-asia-pacific/wave-powered-desalination-riding-high-in-australia.html

Appendix A

Model settings

The settings of the wave model calibrated for the Islandsberg conditions is summarized in Tab. 1.

Table 1: The Islandsberg model set-up of MIKE 21 SW.

Model section	**Model setting / parameter**	**Value**
Simulation period	2005-01-01 - 2009-12-31, 15 minute output	
Discretization	25 frequencies ($f = 0.05 * 1.12^{(n-1)}$, where n is frequency number), 24 directions (15° bins)	
Time step	0.5 - 300 s	
Water level	Temporally and spatially varying	
Current conditions	Not included	
Diffraction	Not included	
Wave breaking	Gamma	0.8
Bottom friction	Nikuradse roughness	0.04
White capping	C_{dis}	2.5
	δ_{dis}	0.25

Calibration

The parameters investigated to optimize the model set-up for Islandsberg is presented in Tab. 2.

Table 2: The MIKE 21 SW parameter values evaluated for calibrating the Islandsberg model set-up.

Model section	**Model setting / parameter**	**Value**
Calibration period	2008-02-12 - 2008-02-25, 15 minute output	
Directional resolution	Number of directions	16 (22.5° bins) 24 (15° bins)
Frequency resolution	Ffactor	1.1 1.11 1.12 1.13 1.14 1.15
	Minimum frequency	0.045 0.05 0.055
Wave breaking	Gamma	0.8 (default) 1 1.2 1.3 1.7
Bottom friction	Nikuradse roughness	0.001 0.005 0.01 0.04 (default)
White capping	C_{dis}	2 2.5 3 4.5 (default)
	δ_{dis}	0.1 0.2 0.25 0.3 0.4 0.5 (default)